

Abstract

We evaluate terrestrial net ecosystem-atmosphere exchange (NEE) of CO₂ from nine global inversion systems that inferred fluxes from four CO₂ observational sources. We use 98 flights in the central and eastern U.S. from the ACT-America aircraft mission to conduct this sub-continental, seasonal-scale evaluation. We use Lagrangian particle dispersion modeling (FLEXPARTv10.4-ERA-Interim) to compare observed and simulated regional biogenic CO₂ mole fractions. We find a positive bias (modeled CO₂ > observed) in the summer and negative bias (modeled CO₂ < observed) in dormant seasons across most flux products, suggesting that the seasonal strength of CO₂ NEE is underestimated in these inverse models. Fluxes inferred from OCO-2 v9 satellite land nadir/glint observations yield an error level that is similar to fluxes inferred from in-situ data. Large bias errors are observed in the croplands and eastern forests. Future experiments are needed to determine if these seasonal biases are associated with biases in net annual flux estimates.

Plain Language Summary

The quantification of terrestrial net ecosystem-atmosphere exchange (NEE) of CO₂ is important to our understanding of the carbon cycle and constitutes an important contribution to the science which underpins climate policy. We use multi-season aircraft observations to evaluate the estimates of seasonal, regional NEE of CO₂ derived from both satellite and ground-based observations of atmospheric CO₂ using nine different global data analysis systems. Our analysis focuses on terrestrial ecosystems in the central and eastern United States. We find that nearly every analysis model yields an underestimate of the seasonal strength of NEE of CO₂ (net photosynthesis too weak in the summer; respiration too weak in the winter) regardless of the CO₂ data source. Additional study is needed to determine both the cause of these seasonal biases, and the impact of this bias on annual net CO₂ flux estimates.

1 Introduction

Accurate, spatially- and temporally- resolved carbon flux estimation is essential for improving climate projections and informing carbon management and policy (e.g., Arora et al., 2020; Millar et al., 2017). A thorough knowledge of the biological CO₂ fluxes from a variety of ecosystems across different geographic locations facilitates total carbon flux estimation and the establishment of national and state implementation plans (e.g., Pan et al., 2011; Tan et al., 2015; J. B. Miller et al., 2020; Wang et al., 2020)(California’s Natural and Working Lands (NWL) Implementation Plan:<https://ww2.arb.ca.gov/our-work/programs/natural-and-working-lands>) . Ecosystem carbon-stock inventories and terrestrial biogeochemical models are commonly used to provide biospheric carbon fluxes for policy planning (e.g., Tan et al., 2015)(California’s NWL Inventory:<https://ww2.arb.ca.gov/nwl-inventory>). Atmospheric inversion of CO₂ mole fraction observations to estimate biospheric CO₂ fluxes is an important and complementary avenue for independent evaluation of ecosystem carbon flux estimates (e.g., Ciais et al., 2010; Chevallier, 2021). These methods have benefited from the expansion of long-term atmospheric observing systems including both ground-based, airborne and space-based platforms (Crisp et al., 2008; Andrews et al., 2014; Sweeney et al., 2015; Karion et al., 2020).

An atmospheric inversion of CO₂ mole fractions optimizes CO₂ fluxes in such a way that simulated atmospheric CO₂ mole fractions agree better with observations (e.g., Rayner et al., 2019). Gridded global CO₂ fluxes are available from several multi-year atmospheric inversions, many of which are frequently updated to quantify CO₂ surface fluxes (e.g., CarbonTracker, <https://www.esrl.noaa.gov/gmd/ccgg/carbontracker/> or the Copernicus Atmosphere Monitoring Service, <https://ads.atmosphere.copernicus.eu/cdsapp#!/dataset/cams-global-greenhouse-gas-inversion>). The inversion models use prior

79 CO₂ flux estimates of different source components, including fossil fuel, biosphere, fire,
80 and ocean. In general, most global inversion systems optimize the magnitude of land bio-
81 spheric and oceanic CO₂ flux terms while leaving fossil fuel emissions “fixed” to derive
82 the optimal solution.

83 These CO₂ flux inversions estimate fluxes across the globe with a variety of spa-
84 tial resolutions. Accurate regional flux information has the potential to inform policy
85 planning and carbon management. To date, regional flux estimates within global inver-
86 sions have shown large differences (Peylin et al., 2013; Crowell et al., 2019). Rigorous
87 evaluation of current CO₂ flux inversion products in time and space is needed to improve
88 atmospheric inversions to the point of being a sound, verified source of information to
89 be used in regional carbon accounting.

90 Aircraft field campaigns are well-suited for regional flux evaluation. Aircraft field
91 campaigns have been deployed in many different regions to investigate CO₂ NEE sur-
92 face fluxes, including the CO₂ Budget and Rectification Airborne study over temperate
93 North America (COBRA) (Gerbig et al., 2003), the Arctic-Boreal Vulnerability Exper-
94 iment in boreal North America (ABoVE) (C. E. Miller et al., 2019), and the Atmospheric
95 Carbon and Transport-America Earth Venture Suborbital mission (ACT-America) (Davis
96 et al., 2021). Several studies have been conducted to evaluate the global CO₂ flux in-
97 versions using independent aircraft CO₂ measurements above the atmospheric bound-
98 ary layer (ABL) and focus on a large domain, such as global or continental scale (Liu
99 & Bowman, 2016; Chevallier et al., 2019; Gaubert et al., 2019; Liu et al., 2021). To date,
100 few studies have been conducted to evaluate the seasonal and sub-continental estimates
101 of the global CO₂ flux inversions. ACT-America is the largest carbon-centric aircraft mis-
102 sion conducted in any midlatitude, continental environment. The multi-seasonal ACT-
103 America campaigns were held in the central and eastern United States (U.S.) during Sum-
104 mer 2016, Winter 2017, Fall 2017, Spring 2018, and Summer 2019 (Davis et al., 2021;
105 Wei et al., 2021). Over 1140 flight hours of data, roughly 45% of which were within ABL,
106 were collected over the course of 121 research flights distributed across the central and
107 eastern United States. The ACT-America flights sampled CO₂ mole fractions from the
108 ABL to the upper free troposphere and were oriented to capture synoptic weather pas-
109 sages typical of each season and region (Pal et al., 2020; Wei et al., 2021). This multi-
110 seasonal weather-oriented aircraft campaign provides a unique opportunity to assess in-
111 verse estimates of regional CO₂ NEE.

112 Global CO₂ flux inversions can be based on ground-based CO₂ monitoring or satellite-
113 based retrievals of the total column CO₂ (XCO₂) mole fractions. These observing sys-
114 tems provide complementary temporal and spatial representativeness. The Orbiting Car-
115 bon Observatory-2 (OCO-2) satellite was launched in July 2014 and was designed to quan-
116 tify sources and sinks of CO₂ across the globe (Eldering et al., 2017). The OCO-2 v9 model
117 intercomparison project (MIP) (Peiro et al., 2021) produced a suite of multiyear (2015-
118 2019) gridded global CO₂ flux inversion products, including the NEE of CO₂. The OCO-
119 2 v9 MIP includes 10 global CO₂ data assimilation systems and is designed to assim-
120 ilate both CO₂ in-situ data and the OCO-2 v9 column CO₂ data individually or collec-
121 tively. We take advantage of the large spatial coverage and multi-seasonal sampling of
122 ACT-America to evaluate the OCO-2 v9 MIP CO₂ NEE of temperate North America
123 by comparing observed ABL CO₂ mole fractions to the corresponding simulated CO₂
124 mole fractions using the series of OCO-2 v9 MIP CO₂ flux inversion products. We ap-
125 ply two evaluation metrics to quantify the errors in CO₂ NEE from commonly-used global
126 CO₂ inversion systems (applied in the OCO-2 v9 MIP) with respect to the independent
127 airborne observations at sub-continental and ecoregional scales. The results are presented
128 in Section 3, after the description of our data and methods in Section 2. The discussions
129 and conclusion are shown in Section 4.

2 Data and methods

2.1 CO₂ NEE flux inversion products

OCO-2 v9 MIP released a suite of ten gridded CO₂ flux inversion products at the global scale encompassing the years 2015-2018. The different inversion systems are standardized in the sense that they are required to assimilate the same four sets of atmospheric observations and use the same fossil fuel CO₂ emissions as part of the inversion system inputs. The ten global CO₂ data assimilation systems are described by Peiro et al. (2021); Zhang et al. (2021) and some additional information are given in Text S1. The four observational data sources include the CO₂ mole fraction measurements from 1) in situ data (IS) compiled in the GLOBALVIEW+ 5.0 (Cooperative Global Atmospheric Data Integration Project, 2019) and NRT v5.1 (CarbonTracker Team, 2019) ObsPack products; 2) the land nadir/land glint (LNLG) retrievals of column-integrated CO₂ from OCO-2 v9; 3) OCO-2 ocean glint (OG) v9 retrievals; and 4) a combination of the in situ and satellite data (LNLGOGIS). The suite of multiyear gridded CO₂ flux inversions are the monthly averaged products (https://gml.noaa.gov/ccgg/OC02_v9mip/). In this study, ancillary gridded global CO₂ NEE products at 3-hourly resolution from nine members of OCO-2 v9 MIP (Text S1) was created for the four ACT-America Campaign periods (summer 2016, winter 2017, fall 2017, and spring 2018). All models in OCO₂ v9 MIP were required to use the same fossil fuel inventory from the Open-source Data Inventory for Anthropogenic CO₂ (ODIAC) 2018 version but were not limited in their choice of biospheric, oceanic and fire prior fluxes. The prior flux inputs for the components of the biospheric, oceanic, and fire sources are listed in Table S2. Overall, there are 7 different prior NEE of CO₂ estimates used in these inversion systems, 6 different prior estimates of the oceanic CO₂ fluxes, and 4 different prior fire CO₂ emissions estimates.

2.2 Influence functions

We established the source-receptor relationship between CO₂ NEE fluxes and atmospheric CO₂ enhancement/depletion along flight tracks using the Lagrangian particle dispersion modeling technique (e.g., Cui et al., 2021). In the study, we aggregated the ACT-America CO₂ measurements in the ABL, excluding take-off and landing portions, to the 10-minute intervals to match the spatial resolution of the transport simulations in the global inversion systems. The ABL determination is described in Pal et al. (2020) and Davis et al. (2021). Each of the 10-minute (roughly 60-70 km at typical flight speeds) intervals is treated as a receptor and we release 1000 particles per receptor and simulate their backward transports for 10 days using FLEXPART v10.4 (“FLEXible PARTicle dispersion model”) (Pisso et al., 2019). The FLEXPART model was driven by the ERA-interim reanalysis data (0.75 x 0.75 degree, 6-hourly).

2.3 Background values

To determine the background values, we sampled the CO₂ mole fraction field at the locations in time and space when and where the particle trajectories’ 10-day backward simulations terminated. The CO₂ mole fraction fields are from the long-term forward simulation from each OCO-2 v9 MIP model within the optimized fluxes from each experiment. The total number of the CO₂ mole fraction fields used here are 35 (9 models and 4 experiments, and the CSU model did not implement the LNLGOGIS experiment).

Specifically, we use the option of FLEXPART to output the spatially and temporally resolved sensitivity field (dimensionless and the range is from 0 to 1) of each receptor used in the study to the initial conditions, interface with the CO₂ mole fraction fields when and where particles are terminated to determine the background value for each receptor (Text S1 and Figure S1).

179

2.4 Evaluation metrics

180

181

182

183

184

185

186

187

188

189

190

191

192

193

194

195

196

197

198

199

We convolve each CO₂ NEE flux product to the atmospheric mole fractions along the ACT-America ABL flight tracks and compare them with the enhancement or depletion levels of the NEE-related CO₂ mole fractions within the ABL observed by ACT-America. The enhancement/depletion levels of the CO₂ mole fractions sampled by ACT-America flights are total CO₂ influenced by different CO₂ sources. The influence of biological sources dominates the aircraft data because the flights were designed to fly over the ecosystems in the Central and Eastern US. We obtain the enhancement/depletion levels of the NEE-related CO₂ mole fractions along flights after extracting the portions influenced by the fossil fuels, fire and ocean from the total CO₂ measurements, as well as the determined regional background values described in Section 2.3 (Cui et al., 2021). The influences of fossil fuels, fire and ocean are calculated using the influence function to convolve their surface fluxes within the 10-day span. We use the fossil fuel CO₂ emission estimates from the ODIAC 2018 emission inventory, and fire emissions from the GFED v4.1s wildfire emission inventory for all cases. The ocean CO₂ influence is derived from the convolution of the influence function and the monthly-averaged posterior oceanic CO₂ flux estimates from each experiment of the individual model in OCO-2 v9 MIP. In the study, we only used the boundary-layer CO₂ mole fractions of the ACT-America flights in the evaluation. Numerical estimates in Cui et al. (2021) show that the fire and ocean fluxes have very small contributions to the ABL mole fractions. Fossil fuel sources have a more significant, but moderate impact.

200

201

202

203

204

205

206

Cui et al. (2021) used the root-mean-square error (RMSE) metric (equation 2) to evaluate inversion products of the CarbonTracker model, one of OCO-2 v9 MIP ensemble members, based on the comparisons between the simulated and ACT-America referenced NEE-related CO₂ mole fractions. In this study, we apply the RMSE metric to nine models of OCO-2 v9 MIP. Furthermore, we focus more on the mean bias error (MBE) metric analysis (equation 3) in the CO₂ mole fraction space to investigate the bias error of each inversion case in OCO-2 v9 MIP.

$$RMSE = \frac{\sum_{i=1}^N \sqrt{(y_{modbio_i} - y_{ACTbio_i})^2}}{N} \quad (1)$$

$$MBE = \frac{\sum_{i=1}^N (y_{modbio_i} - y_{ACTbio_i})}{N} \quad (2)$$

207

208

209

210

211

212

213

, where i denotes each receptor, and N denotes the number of receptors. More details of y_{modbio_i} and y_{ACTbio_i} are described in Cui et al. (2021). Similar to Cui et al. (2021), our evaluation is seasonal. The RMSE and MBE values are calculated for each campaign (i.e each season). The flux product associated with smaller RMSE values indicates better spatially and temporally resolved flux estimates. The MBE analysis is also applied for each campaign. Smaller biases imply NEE of CO₂ that is most consistent with the mean impact of biogenic fluxes on ABL CO₂.

214

2.5 Ecoregion-based evaluation framework

215

216

217

218

219

220

To evaluate fluxes by ecoregion, we group the receptors by ecoregion and calculate the MBE values between the simulated and observed biological CO₂ mole fractions for each group. The ecoregion-based MBE analysis are subsets of the overall MBE analysis. We present the “zoom-in” maps to investigate the spatial origins of the MBE values and show the maximum MBE value for each ecoregion associated with the corresponding inversion case.

221

222

We attribute the receptors along the flight tracks to different ecoregions, taking advantage of the source-receptor relationship obtained from the Lagrangian framework. Specif-

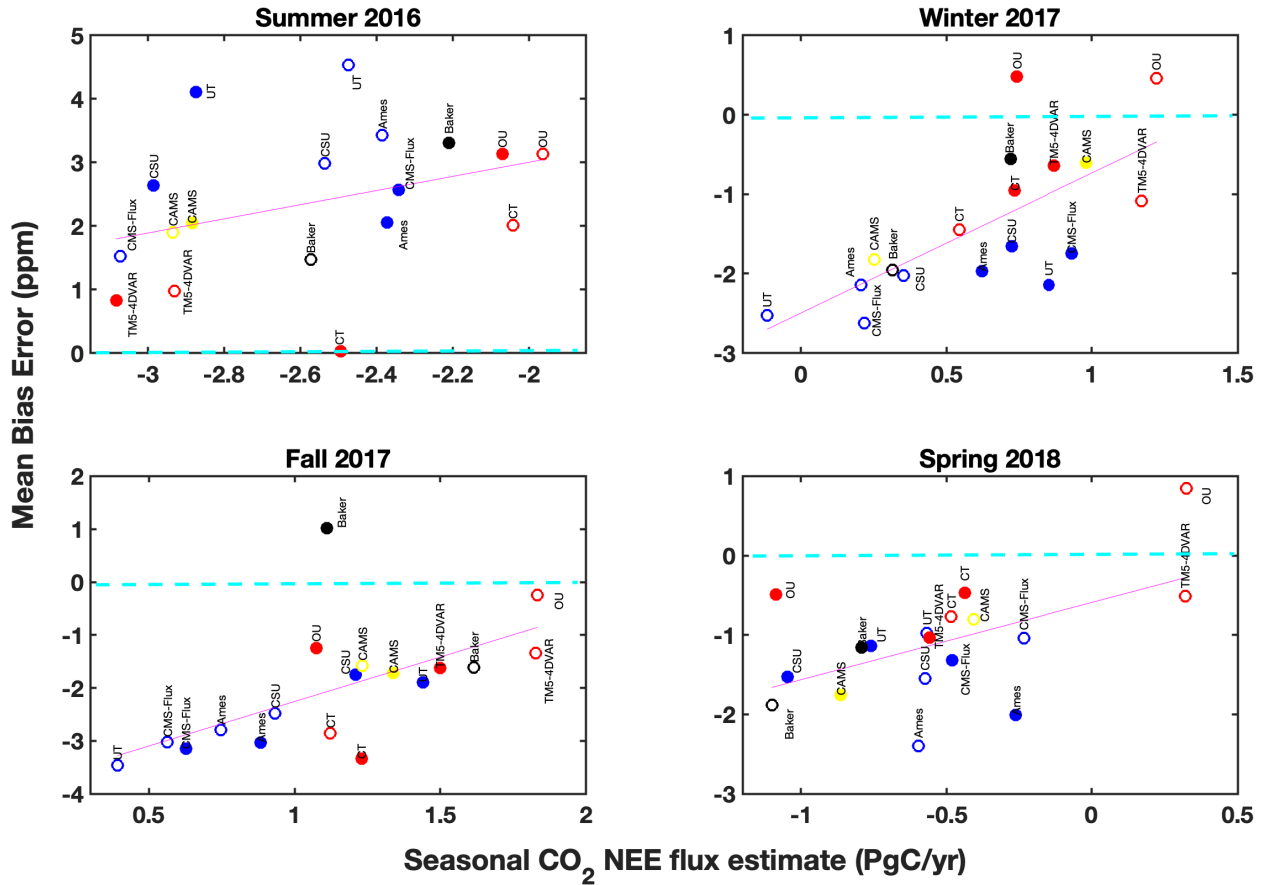


Figure 1. Seasonal NEE of CO₂ estimated from OCO-2 v9 MIP in Central and Eastern US (Text S1 and Figure S1) as a function of seasonal Mean Bias Error (MBE) values in posterior fluxes from the OCO- 2 v9 -MIP calculated using ACT-America ABL CO₂ mole fraction observations and a Lagrangian particle dispersion model (Cui et al., 2021). The observations and calculated NEE of CO₂ encompass July-August 2016 (“Summer 2016”); February-March 2017 (“Winter 2017”); October-November 2017 (“Fall 2017”); and April-May 2018 (“Spring 2018”). The open circles denote the IS experiments, and the solid circles denote the LNLG experiments. The TM5 group (CT, OU, and TM5-4DVAR) is colored in red, the GEOS-Chem group (Ames, CMS-Flux, UT, and CSU) is colored in blue, the Baker model is in black, and the CAMS model is in yellow. The pink lines are linear regressions of all cases for each season.

223 ically, we attribute each receptor to one eco-region which contributes the largest influ-
 224 ence function for that receptor (Text S1 and Figure S2). We group the segments of CO₂
 225 mole fractions along the flight tracks into different ecoregions and apply the MBE anal-
 226 ysis for each group to investigate the associated seasonal bias levels aligned with the ecore-
 227 gion regions of the temperate North America area. The overall spatial coverages of the
 228 influence functions of ACT-America are shown in Cui et al. (2021). We focus on region
 229 1-9 in this study, which contribute largest influence on the enhancement/depletion of CO₂
 230 mole fractions along ACT-America ABL flight tracks.

3 Results

Figure 1 shows seasonal Mean Bias Error (MBE) levels to the seasonal NEE estimation of OCO-2 v9 MIP members. We focus here on the flux estimates from the in-situ (“IS”) and the OCO-2 v9 land nadir/land glint (“LNLG”) experiments, which Cui et al., (2021) suggests are the most reliable NEE estimates for the central and eastern US. We find correlations between OCO-2 v9 MIP seasonal NEE estimates and seasonal MBE. The corresponding correlation coefficient (p-value) to the four campaigns are 0.4 (p=0.15), 0.7 (p=0.001), 0.6 (p=0.009), and 0.5 (p=0.02), respectively. The correlations are statistically significant for the winter, fall and spring months. Figure 1 shows that posterior estimates of NEE of CO₂ are underestimated in the IS and LNLG experiments compared to observations during winter, fall, and spring. Posterior estimates of NEE of CO₂ are overestimated (not sufficiently negative) during the summer. The TM5-4DVAR and OU models have the best performance during winter and fall seasons. The TM5-4DVAR and CT model within the LNLG experiment have the best performance during the summer.

The inversion products from each model are only required to use the same fossil fuel emission and the same observational datasets, leaving many potential differences among the inversion systems including prior fluxes, transport, and inversion algorithms. Therefore, some of the performance differences of the inversion systems is caused by the differences of these model framework components, enabling limited diagnosis of the causes of the MBEs. Overall, the TM5-4DVAR model has the best performance across the different seasons. The TM5 group shows the best performance among the transport models, with smaller MBEs than the other transport models across four seasons. The OCO-2 v9 land nadir/land glint experiment yields the MBE level that is similar to, or better (e.g winter) than, the in situ data experiment. We have used one transport model to create the influence functions used to link NEE of CO₂ to ABL CO₂ mole fractions (see Section 2), thus we compare all of the systems on an equivalent basis. It is possible, however, that a bias in our influence functions contributes to the MBE in Figure 1, and yields incorrect rankings among these inversions.

In summary, we find the NEE of CO₂ in central and eastern North America by nearly all these inversion systems to be positively biased in summer and negatively biased in the other three seasons, with the degree of bias varying across the inversion system. Therefore, the magnitude of the seasonal cycle of NEE of CO₂ across central and eastern Temperate North America is likely to be underestimated across the models in the OCO-2 v9 MIP. The overall annual bias from these systems is not clear, since the seasonal flux biases change sign and will cancel out over the course of a year to a degree that is not clear from this analysis.

A number of broad patterns emerge when the MBE is evaluated for each ecoregion (Figure 2). In all seasons the patterns of ecoregion MBEs change relatively little as a function of the data source used in the inversion. Summer and fall have the largest overall MBEs. The large MBEs are located in the Appalachian forests (ecoregion 5), central crops and forest (ecoregion 6), the corn belt (ecoregion 7), and the northern crops (ecoregion 8). More pronounced MBE levels in the positive and negative direction are found in the Baker and UT models, which may imply a smaller model-data-mismatch covariance given in the model than others. The OU model MBE most often diverges in sign from the other models during the dormant season, and the Ames and CMS-Flux models often have the largest negative MBEs in the dormant seasons, especially when limiting the discussion to the IS and LNLG inversions.

During the summertime, we identify large positive biases in Appalachian forests (ecoregion 5), central crops and forests (ecoregion 6), the corn belt (ecoregion 7), and northern crops (ecoregion 8). The UT and Baker-mean models contain many of the peak positive biases across these ecoregions. The TM5-4DVAR model shows the smallest MBE

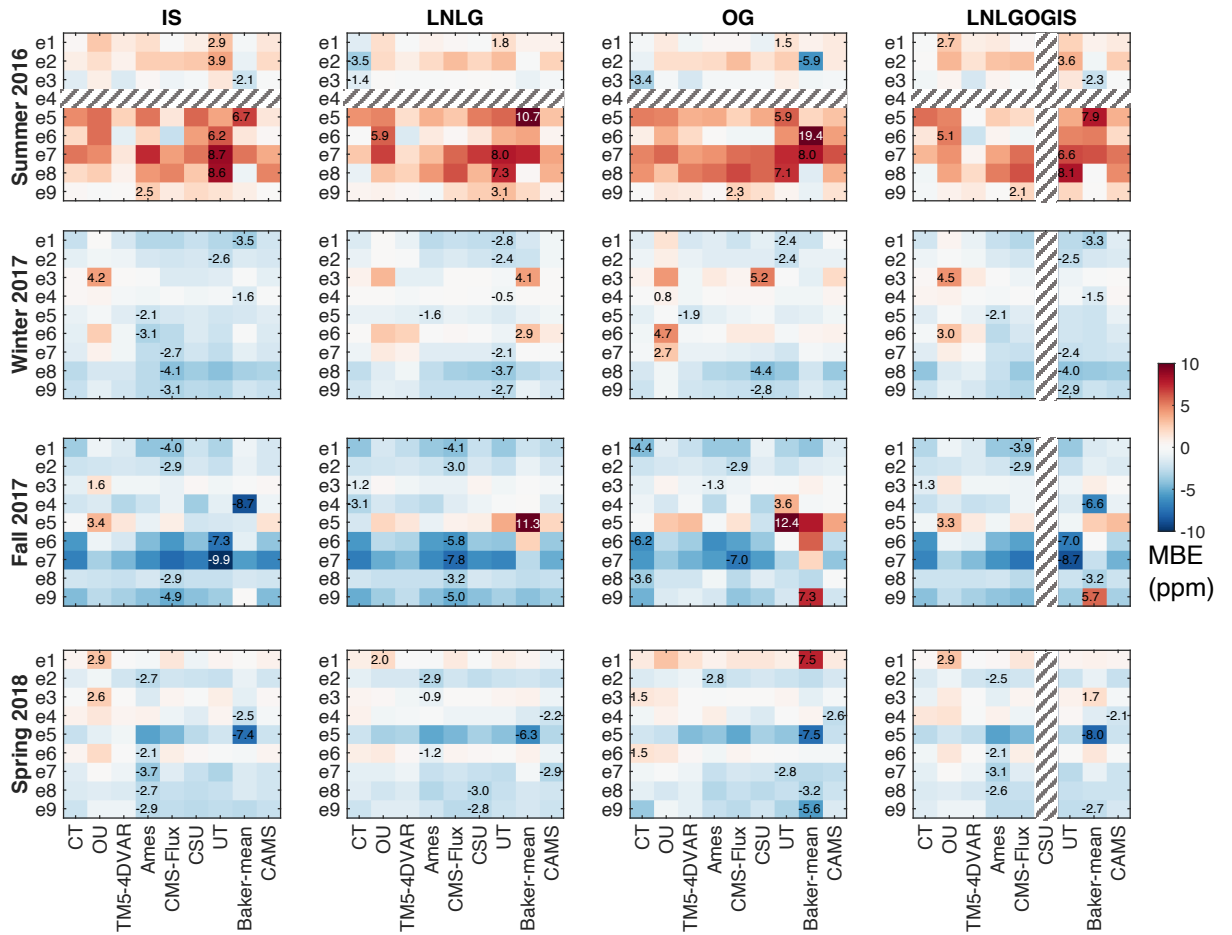


Figure 2. Mean Bias Error (MBE, ppm) for 9 different ecoregions in Central and Eastern Temperate North America. The largest magnitude of MBE for each ecoregion is written onto the cell. A warm color denotes a positive bias, and a cold color denotes a negative bias. The ecoregions are defined in Figure 2. Shaded areas denote no data.

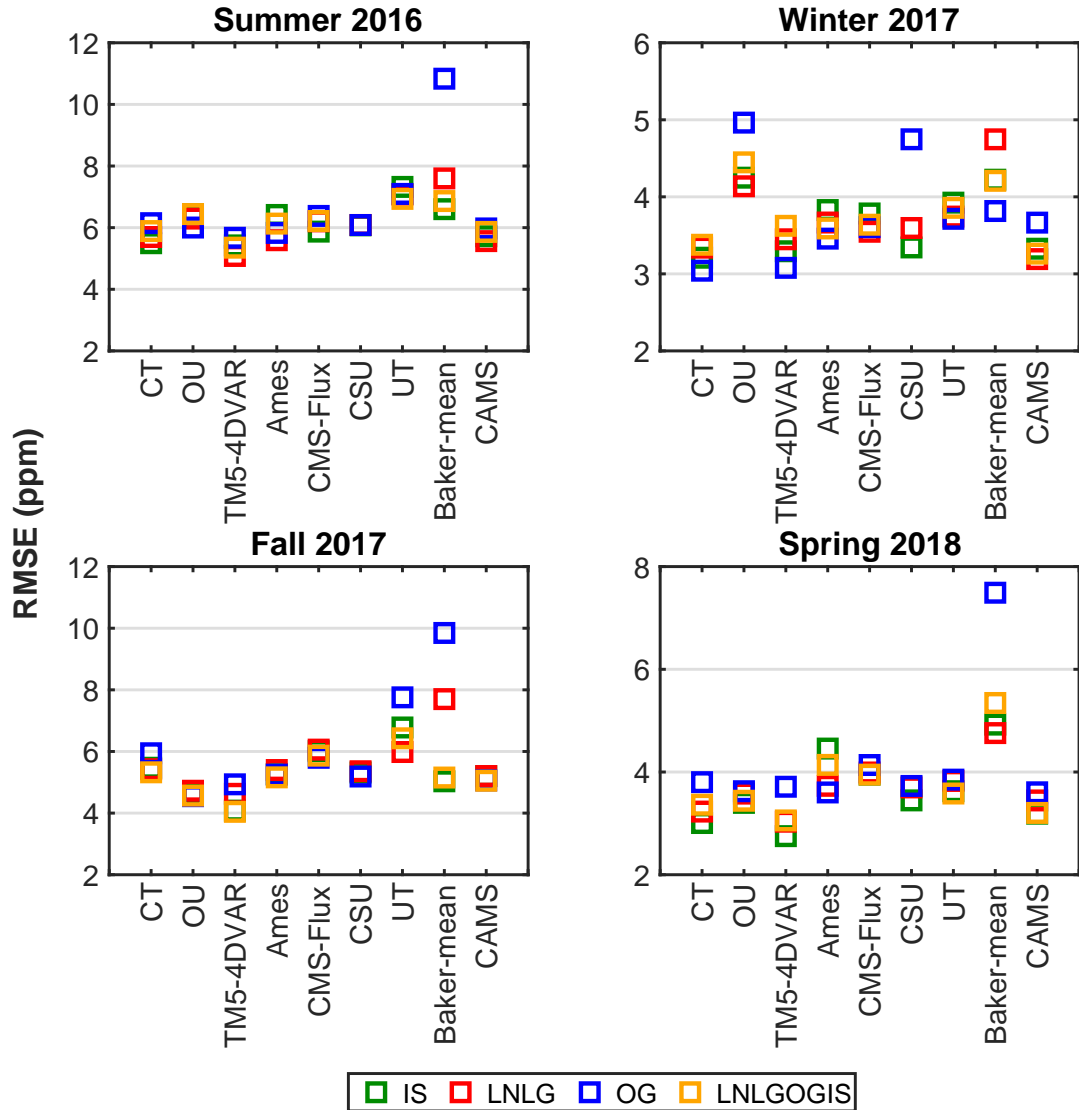


Figure 3. RMSE of the posterior biogenic CO₂ computed from all inverse estimates of NEE of CO₂ compared to the observed ABL CO₂ mole fractions from each of four seasonal ACT-America campaigns.

283 across all ecoregions. During the fall months, large negative MBE values are found in
 284 most ecoregions with the exception of the Appalachian forests (ecoregion 5) where the
 285 MBEs are positive. The Baker model again stands out in comparison to other inversion
 286 systems, with positive MBEs for many ecoregions when driven by OCO-2 data (i.e., LNLG
 287 and OG). Given that only moderate NEE of CO₂ is expected in the fall, the performance
 288 of the OCO-2 v9 MIP models during the fall months is relatively poor compared to other
 289 seasons.

290 Figure 3 and Figure 4 show the RMSE and MBE analysis, respectively, for four
 291 data experiments in OCO-2 v9 MIP including IS, LNLG, the OCO-2 v9 ocean glint (“OG”)
 292 experiment, and the combination of IS, LNLG and OG experiment (“LNLGOGIS”) (see
 293 details in section 2).

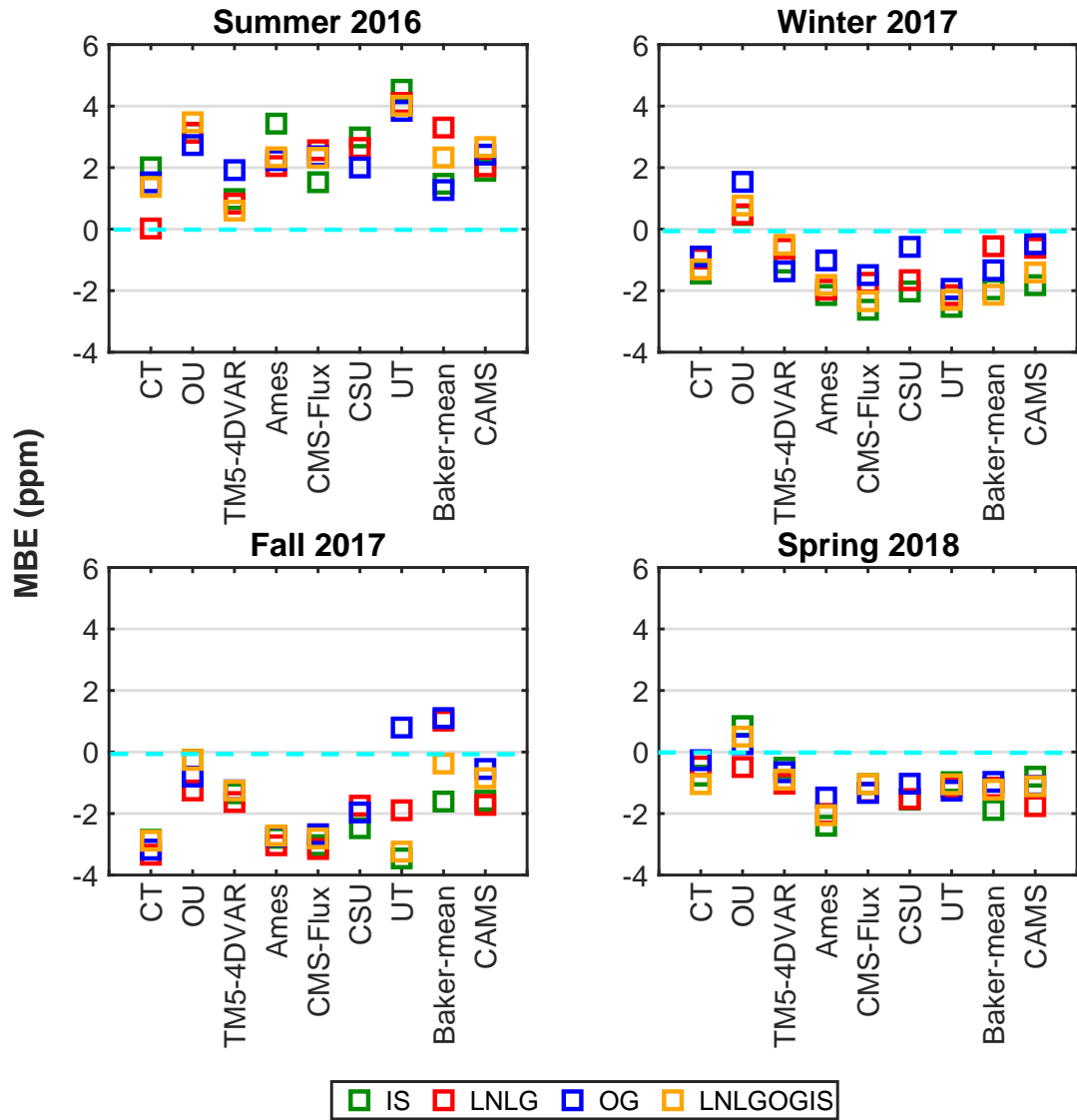


Figure 4. MBE of the posterior biogenic CO₂ computed from all inverse estimates of NEE of CO₂ compared to the observed ABL CO₂ mole fractions from each of four seasonal ACT-America campaigns.

294 The RMSE analysis (Figure 3) shows seasonal patterns likely related to flux mag-
 295 nitudes. Across all members of OCO-2 v9 MIP, spring and winter CO₂ NEE flux esti-
 296 mates have smaller RMSE levels than fall and summer estimates. The variability of RMSE
 297 levels across different models is small during the spring months, and largest during the
 298 fall months. These findings are roughly consistent with larger NEE (Figure 1 and Fig-
 299 ure S4-7), hence larger potential for model-data differences, in the more biologically ac-
 300 tive seasons.

301 Sensitivity of RMSE in the CO₂ NEE flux estimates to data sources varies, per-
 302 haps indicative of the construction of the inversion systems. Most of the models in the
 303 OCO-2 v9 MIP are not strongly sensitive to changes in the observational source. The
 304 Baker-mean model, in contrast, is relatively sensitive to the source data used in the in-
 305 version, especially to the OCO-2 ocean glint v9 retrievals (“OG”). The OU and CSU mod-
 306 els are sensitive to the OG data during the wintertime as well. The UT model is sen-
 307 sitive to the different observing datasets during the fall months. This suggests that these
 308 inversion systems are the most data driven. In addition, RMSE analyses suggest that
 309 the OCO-2 v9 OG-based inversion is inferior to other experiments, yielding the highest
 310 RMSE across seasons and models.

311 The MBE analysis as a function of the observational data set shows similar pat-
 312 terns (Figure 4) to the RMSE analysis. MBE levels are smaller in winter and spring months
 313 than the fall and summer months, and the MBE level is smallest in the spring. Unlike
 314 the RMSE analysis, the OG experiments here don’t show the large discrepancies as com-
 315 pared to the other experiments. During the fall months, the MBE levels for the CO₂ NEE
 316 flux estimates from the UT and Baker model still display large divergences across dif-
 317 ferent observing datasets. The LNLGOGIS experiment includes both in situ and OCO-
 318 2 data but we do not find superior performance in the current global inversion system
 319 despite the superior data density. Patterns of MBE across models and regions have been
 320 discussed earlier in the paper.

321 4 Discussions and Conclusion

322 We implement a regional evaluation of net ecosystem exchange (NEE) of CO₂ flux
 323 products from nine current state-of-the-science global inversion systems in central and
 324 eastern temperate North America, using the largest carbon-centric, regional-scale air-
 325 craft mission (ACT-America) yet deployed anywhere on the earth. We estimate the sea-
 326 sonal performance of CO₂ NEE flux products of the OCO-2 v9 MIP across this portion
 327 of North America and expand the evaluation to the ecoregions within the domain.

328 The seasonal bias analysis shows that the inversion models’ NEE estimates are pos-
 329 itively biased in summer, and negatively biased in winter, fall, and spring across most
 330 flux products, suggesting that the seasonal magnitude of CO₂ NEE is underestimated
 331 in these global CO₂ inversion systems. The performance of the OCO-2 v9 land nadir/land
 332 glint data experiment is similar to the in situ experiment, an encouraging finding for re-
 333 gions of the world where the in situ observing network is sparse. The spatially resolved
 334 errors for the regional fluxes in the inversion models are not strongly dependent on the
 335 observational data sources for most of the models but a small number of the inversion
 336 systems display noticeably greater sensitivity to the data source. Large seasonal MBE
 337 values exist in the crop land and eastern forest regions.

338 The implication that most OCO-2 v9 MIP models underestimate the seasonal am-
 339 plitude of NEE across central and eastern US ecosystems, regardless of data set, is strik-
 340 ing. Similar results were found in two additional studies using ACT-America observa-
 341 tions. Zhang et al. (2021) compared the posterior CO₂ 4D fields from different inversion
 342 systems of OCO₂ v9 MIP to the ACT-America flight observations to understand the weather-
 343 driven atmospheric CO₂ differences, which does not separate the impacts of transport

344 and flux errors. Zhang et al. (2021) found that most inversion systems in most seasons
 345 underestimated the difference in CO₂ between the ABL and the free troposphere, a re-
 346 sult that is potentially consistent with systematically underestimated seasonal flux mag-
 347 nitudes. It is worth noting that the methods of Zhang et al. (2021) do not depend on
 348 a "third-party" atmospheric transport model to project mole fractions into flux space,
 349 as was done in this study. Feng et al. (2021) found a systematic underestimate of sum-
 350 mer 2016 net uptake of CO₂ when comparing an ecosystem flux ensemble and Carbon-
 351 Tracker posterior fluxes to ACT-America and NOAA tall tower CO₂ observations. The
 352 results of Feng et al. (2021) use a WRF-Chem atmospheric ensemble to transport flux
 353 estimates, presenting a third and independent treatment of atmospheric transport yet
 354 yielding similar findings, albeit only for the summer season. Finally, Hu et al. (2019) used
 355 independent aircraft vertical profiles of CO₂ to evaluate CarbonTracker's CO₂ NEE in-
 356 version products and show similar seasonal-biases pattern in terms of simulating the ABL
 357 CO₂ mole fractions.

358 The impact of this apparent underestimate in the seasonal cycle of fluxes on an-
 359 nually integrated NEE of CO₂ of North America is not clear but deserves additional in-
 360 vestigation. It is also possible that this seasonal bias could directly impact or is indica-
 361 tive of features of these inversions that could impact NEE estimates in other regions of
 362 the globe. The finding that the TM5-based inversions appear on average to have smaller
 363 seasonal biases than the GEOS-Chem-based inversions is also potentially consistent with
 364 the findings of Schuh et al. (2019). Schuh et al. (2019) suggested that TM5 mixes more
 365 vigorously in the vertical than GEOS-Chem. This could lead to TM5-based inversions
 366 requiring stronger NEE of CO₂ to match ABL CO₂ observations, since seasonal fluxes
 367 would be diluted within a larger atmospheric mixing volume. Schuh et al. (2019) showed
 368 that, globally, these differences in atmospheric mixing led to large differences in inverse
 369 estimates of annual NEE of CO₂. We suggest that continued understanding of the causes
 370 of the biases at sub-continental scales found in this study will enable increased confidence
 371 not just in regional, seasonal NEE, but in global, annual NEE estimates.

372 Acknowledgments

373 The ACT-America project is a NASA Earth Venture Suborbital 2 project funded by NASA's
 374 Earth Science Division. We would like to acknowledge the NASA grants: NNX15AG76G
 375 to Penn State and NNX15AJ07G to Colorado State, and the support for the OCO-2 v9
 376 flux model inter-comparison project provided through NASA grant #80 NSSC 18K0909.
 377 MJ acknowledges the internal funding from NASA's Earth Science Research and Anal-
 378 ysis Program . We also would like to acknowledge NASA's Earth System Science Pathfinder
 379 Program Office, NASA's Airborne Sciences Program, NASA's Atmospheric Science Data
 380 Center, and NASA's Pleiades supercomputing facilities. All ACT-America in situ data
 381 used in the manuscript can be found at the ORNL DAAC ([https://daac.ornl.gov/](https://daac.ornl.gov/actamerica)
 382 [actamerica](https://daac.ornl.gov/actamerica)). The FLEXPART v10.4 model can be found online ([https://www.flexpart](https://www.flexpart.eu/wiki/FpInstall)
 383 [.eu/wiki/FpInstall](https://www.flexpart.eu/wiki/FpInstall)). The authors declare, to their knowledge, no conflicts of inter-
 384 est with the submission of this manuscript.

385 References

- 386 Andrews, A. E., Kofler, J. D., Trudeau, M. E., Williams, J. C., Neff, D. H., Masarie,
 387 K. A., ... Tans, P. P. (2014). Co₂, co, and ch₄ measurements from tall towers
 388 in the noaa earth system research laboratory's global greenhouse gas refer-
 389 ence network: instrumentation, uncertainty analysis, and recommendations for
 390 future high-accuracy greenhouse gas monitoring efforts. *Atmospheric Measure-*
 391 *ment Techniques*, 7(2), 647–687.
- 392 Arora, V. K., Katavouta, A., Williams, R. G., Jones, C. D., Brovkin, V., Friedling-
 393 stein, P., ... Ziehn, T. (2020). Carbon-concentration and carbon-climate
 394 feedbacks in cmip6 models and their comparison to cmip5 models. *Biogeo-*

- 395 *sciences*, 17(16), 4173–4222. Retrieved from [https://bg.copernicus.org/](https://bg.copernicus.org/articles/17/4173/2020/)
 396 [articles/17/4173/2020/](https://bg.copernicus.org/articles/17/4173/2020/) doi: 10.5194/bg-17-4173-2020
- 397 Chevallier, F. (2021). Fluxes of carbon dioxide from managed ecosystems estimated
 398 by national inventories compared to atmospheric inverse modeling. *Geophys-*
 399 *ical Research Letters*, 48(15), e2021GL093565. doi: [https://doi.org/10.1029/](https://doi.org/10.1029/2021GL093565)
 400 [2021GL093565](https://doi.org/10.1029/2021GL093565)
- 401 Chevallier, F., Remaud, M., O’Dell, C. W., Baker, D., Peylin, P., & Cozic, A.
 402 (2019). Objective evaluation of surface- and satellite-driven carbon dioxide
 403 atmospheric inversions. *Atmospheric Chemistry and Physics*, 19(22), 14233–
 404 14251. doi: 10.5194/acp-19-14233-2019
- 405 Ciais, P., Rayner, P., Chevallier, F., Bousquet, P., Logan, M., Peylin, P., & Ra-
 406 monet, M. (2010). Atmospheric inversions for estimating co2 fluxes: meth-
 407 ods and perspectives. *Climatic Change*, 103(1-2), 69 - 92. Retrieved from
 408 <https://hal.inrae.fr/hal-02665340> doi: 10.1007/s10584-010-9909-3
- 409 Crisp, D., Miller, C. E., & DeCola, P. L. (2008). NASA Orbiting Carbon Obser-
 410 vatory: measuring the column averaged carbon dioxide mole fraction from
 411 space. *Journal of Applied Remote Sensing*, 2(1), 1 – 14. Retrieved from
 412 <https://doi.org/10.1117/1.2898457> doi: 10.1117/1.2898457
- 413 Crowell, S., Baker, D., Schuh, A., Basu, S., Jacobson, A. R., Chevallier, F., ...
 414 Jones, D. B. A. (2019). The 2015–2016 carbon cycle as seen from oco-2 and
 415 the global in situ network. *Atmospheric Chemistry and Physics*, 19(15), 9797–
 416 9831.
- 417 Cui, Y. Y., Jacobson, A. R., Feng, S., Wesloh, D., Barkley, Z. R., Zhang, L., ...
 418 Davis, K. J. (2021). Evaluation of carbontracker’s inverse estimates of
 419 north american net ecosystem exchange of co2 from different observing sys-
 420 tems using act-america airborne observations. *Journal of Geophysical Re-*
 421 *search: Atmospheres*, 126(12), e2020JD034406. doi: [https://doi.org/10.1029/](https://doi.org/10.1029/2020JD034406)
 422 [2020JD034406](https://doi.org/10.1029/2020JD034406)
- 423 Davis, K., Browell, E., Feng, S., Lauvaux, T., Obland, M., Pal, S., ... Williams,
 424 C. A. (2021). The atmospheric carbon and transport (act)-america mis-
 425 sion. *Bull. Amer. Meteorol. Soc.*, 1–54. doi: [https://doi.org/10.1175/](https://doi.org/10.1175/BAMS-D-20-0300.1)
 426 [BAMS-D-20-0300.1](https://doi.org/10.1175/BAMS-D-20-0300.1)
- 427 Feng, S., Lauvaux, T., Williams, C. A., Davis, K. J., Zhou, Y., Baker, I., ... Wesloh,
 428 D. (2021). Joint co2 mole fraction and flux analysis confirms missing processes
 429 in casa terrestrial carbon uptake over north america. *Global Biogeochemi-*
 430 *cal Cycles*, 35(7), e2020GB006914. (e2020GB006914 2020GB006914) doi:
 431 <https://doi.org/10.1029/2020GB006914>
- 432 Gaubert, B., Stephens, B. B., Basu, S., Chevallier, F., Deng, F., Kort, E. A., ...
 433 Yin, Y. (2019). Global atmospheric co₂ inverse models converging on neu-
 434 tral tropical land exchange, but disagreeing on fossil fuel and atmospheric
 435 growth rate. *Biogeosciences*, 16(1), 117–134. Retrieved from [https://](https://bg.copernicus.org/articles/16/117/2019/)
 436 bg.copernicus.org/articles/16/117/2019/ doi: 10.5194/bg-16-117-2019
- 437 Gerbig, C., Lin, J. C., Wofsy, S. C., Daube, B. C., Andrews, A. E., Stephens, B. B.,
 438 ... Grainger, C. A. (2003). Toward constraining regional-scale fluxes of co2
 439 with atmospheric observations over a continent: 1. observed spatial variabil-
 440 ity from airborne platforms. *Journal of Geophysical Research: Atmospheres*,
 441 108(D24). doi: <https://doi.org/10.1029/2002JD003018>
- 442 Hu, L., Andrews, A. E., Thoning, K. W., Sweeney, C., Miller, J. B., Michalak,
 443 A. M., ... van der Velde, I. R. (2019). Enhanced north american carbon
 444 uptake associated with el niño. *Science Advances*, 5(6).
- 445 Karion, A., Callahan, W., Stock, M., Prinzivalli, S., Verhulst, K., Kim, J., ... Whet-
 446 stone, J. (2020). Greenhouse gas observations from the northeast corridor
 447 tower network. *Earth Systems Science Data*.
- 448 Liu, J., Baskaran, L., Bowman, K., Schimel, D., Bloom, A. A., Parazoo, N. C., ...
 449 Wofsy, S. (2021). Carbon monitoring system flux net biosphere exchange

- 450 2020 (cms-flux nbe 2020). *Earth System Science Data*, 13(2), 299–330. doi:
451 10.5194/essd-13-299-2021
- 452 Liu, J., & Bowman, K. (2016). A method for independent validation of surface
453 fluxes from atmospheric inversion: Application to co₂. *Geophysical Research*
454 *Letters*, 43(7), 3502–3508. doi: 10.1002/2016gl067828
- 455 Millar, R., Fuglestvedt, J., Friedlingstein, P., Rogelj, J., Grubb, M., Matthews, H.,
456 ... Allen, M. (2017). Emission budgets and pathways consistent with limiting
457 warming to 1.5 c. *Nature Geoscience*, 10, 741–747.
- 458 Miller, C. E., Griffith, P. C., Goetz, S. J., Hoy, E. E., Pinto, N., McCubbin, I. B.,
459 ... Margolis, H. A. (2019). An overview of ABoVE airborne campaign data
460 acquisitions and science opportunities. *Environmental Research Letters*, 14(8),
461 080201.
- 462 Miller, J. B., Lehman, S. J., Verhulst, K. R., Miller, C. E., Duren, R. M., Yadav,
463 V., ... Sloop, C. D. (2020). Large and seasonally varying biospheric co₂
464 fluxes in the los angeles megacity revealed by atmospheric radiocarbon. *Pro-*
465 *ceedings of the National Academy of Sciences*, 117(43), 26681–26687. doi:
466 10.1073/pnas.2005253117
- 467 Pal, S., K. J. Davis, K. J., Pauly, R. M., McGill, M. J., Campbell, L., & Hoffman,
468 K. (2020). A brief description of the cloud physics lidar-derived atmospheric
469 boundary layer top height data sets obtained using wavelet transform algo-
470 rithm. *ORNL DAACm, Oak Ridge, Tennessee, USA.*
- 471 Pan, Y., Birdsey, R. A., Fang, J., Houghton, R., Kauppi, P. E., Kurz, W. A., ...
472 Hayes, D. (2011). A large and persistent carbon sink in the world's forests.
473 *Science*, 333(6045), 988–993. doi: 10.1126/science.1201609
- 474 Peiro, H., Crowell, S., Schuh, A., Baker, D. F., O'Dell, C., Jacobson, A. R.,
475 ... Baker, I. (2021). Four years of global carbon cycle observed from
476 oco-2 version 9 and *in situ* data, and comparison to oco-2 v7. *Atmo-*
477 *spheric Chemistry and Physics Discussions*, 2021, 1–50. Retrieved from
478 <https://acp.copernicus.org/preprints/acp-2021-373/> doi: 10.5194/
479 acp-2021-373
- 480 Peylin, P., Law, R. M., Gurney, K. R., Chevallier, F., Jacobson, A. R., Maki, T.,
481 ... Zhang, X. (2013). Global atmospheric carbon budget: results from an
482 ensemble of atmospheric co₂ inversions. *Biogeosciences*, 10(10), 6699–6720.
483 doi: 10.5194/bg-10-6699-2013
- 484 Pisso, I., Sollum, E., Grythe, H., Kristiansen, N. I., Cassiani, M., Eckhardt, S.,
485 ... Stohl, A. (2019). The lagrangian particle dispersion model flexpart
486 version 10.4. *Geoscientific Model Development*, 12(12), 4955–4997. doi:
487 10.5194/gmd-12-4955-2019
- 488 Rayner, P. J., Michalak, A. M., & Chevallier, F. (2019). Fundamentals of data
489 assimilation applied to biogeochemistry. *Atmospheric Chemistry and Physics*,
490 19(22), 13911–13932. doi: 10.5194/acp-19-13911-2019
- 491 Schuh, A. E., Jacobson, A. R., Basu, S., Weir, B., Baker, D., Bowman, K., ...
492 Palmer, P. I. (2019). Quantifying the impact of atmospheric transport un-
493 certainty on co₂ surface flux estimates. *Global Biogeochemical Cycles*, 33(4),
494 484–500. doi: <https://doi.org/10.1029/2018GB006086>
- 495 Sweeney, C., Karion, A., Wolter, S., Newberger, T., Guenther, D., Higgs, J. A., ...
496 Tans, P. P. (2015). Seasonal climatology of co₂ across north america from
497 aircraft measurements in the noaa/esrl global greenhouse gas reference net-
498 work. *Journal of Geophysical Research: Atmospheres*, 120(10), 5155–5190. doi:
499 <https://doi.org/10.1002/2014JD022591>
- 500 Tan, Z., Liu, S., Sohl, T. L., Wu, Y., & Young, C. J. (2015). Ecosystem carbon
501 stocks and sequestration potential of federal lands across the conterminous
502 united states. *Proceedings of the National Academy of Sciences*, 112(41),
503 12723–12728. doi: 10.1073/pnas.1512542112
- 504 Wang, J., Feng, L., Palmer, Y., Paul I.and Liu, Fang, S., Bösch, H., O'Dell,

- 505 C. W., ... Xia, C. (2020). Large chinese land carbon sink estimated
506 from atmospheric carbon dioxide data. *Nature*, 586(7831), 720-723. doi:
507 10.1038/s41586-020-2849-9
- 508 Wei, Y., Shrestha, R., Pal, S., Gerken, T., McNelis, J., Singh, D., ... Davis, K.
509 (2021). The atmospheric carbon and transport (act) – america datasets:
510 Description, management, and delivery. *Earth and Space Science*. doi:
511 <https://www.essoar.org/doi/pdf/10.1002/essoar.10505692.1>.
- 512 Zhang, L., Davis, K. J., Schuh, A. E., Jacobson, A. R., Pal, S., Cui, Y. Y., ... Basu,
513 S. (2021). Multi-season evaluation of co2 weather in oco-2 mip models. *Earth
514 and Space Science Open Archive*, 29. doi: 10.1002/essoar.10507526.1